Carbon Dioxide Foaming of Glassy Polymers

M. WESSLING,* Z. BORNEMAN, Th. VAN DEN BOOMGAARD, and C. A. SMOLDERS

P.O. Box 217, University of Twente, 7500 AE Enschede, The Netherlands

SYNOPSIS

The mechanism of foaming a glassy polymer using sorbed carbon dioxide is studied in detail. A glassy polymer supersaturated with nitrogen forms a microcellular foam, if the polymer is quickly heated above its glass transition temperature. A glassy polymer supersaturated with CO_2 forms this foam-like structure at much lower temperatures which indicates the T_g-depressing effect of CO_2. Having this interpretation in mind, the overall sample morphology, i.e., a porous foam enclosed by dense outer skins, can be completely explained. The dense skins, however, are not homogeneous but show a nodular structure when analyzed by SEM and AFM. Foaming experiments with samples having a different thermal history suggest that the nucleation mechanism underlying the foaming process is heterogeneous in nature. © 1994 John Wiley & Sons, Inc.

INTRODUCTION

Microcellular foams prepared from thermoplastic materials were developed to reduce the amount of polymer used in mass produced items.[1] To prepare such foams, a glassy polymer is saturated with a nonreactive gas at high pressures and at room temperature. The pressure is released after gas uptake has reached equilibrium. The specimen remains supersaturated with gas because the release of absorbed gas is slow. If the specimen is now heated above its glass transition temperature, nucleation of the gas phase occurs, and gas bubbles can grow in the matrix due to the drastically increased chain mobility in the rubbery state. A comprehensive, experimental study on nucleation and growth of gas bubbles was carried out by Kumar[2] for the polycarbonate/CO_2 system.

In this article, we will describe how this particular production process for porous glassy polymers can be used as a model to investigate the influence of the absorbed nonreactive gas on the polymer matrix itself. First, we will present a detailed physical and mathematical description of the mass and heat transport phenomena occurring during the preparation process. Experiments and calculations are carried out with the polycarbonate/CO_2 system. Second, we will illustrate that this model provides an easy-to-use method to determine the glass transition temperature depression by absorbed gaseous penetrant molecules. In this case, the experiments were carried out with an aromatic polyimide.

The glass transition temperature depression is of special interest in the processing of thermoplastic materials into foams. During the extrusion process, the dissolved CO_2 strongly influences the viscosity of the polymer melt. The viscosity is related to the difference between the processing temperature and the glass transition temperature by the WLF-equation.[3] The glass transition temperature, however, is not known for the polymer/CO_2 system because the T_g depression is unknown. The T_g depression is also of interest in membrane processes based on the solution–diffusion transport mechanism. In this case, the sorbed penetrant molecules alter the transport properties of the polymer such that the polymer shows reduced selective properties.[4]

In a third part, we will concentrate on the mechanism of the formation. From the literature,[2] it is clear that the nucleation mechanism of the bubbles is not completely understood. Therefore, a number of experiments on the nucleation mechanism of bubbles will be presented using polysulfone as a polymer.

Rather than using the same polymer for all experiments, different problems linked to the foaming

* To whom correspondence should be addressed.

Journal of Applied Polymer Science, Vol. 53, 1497–1512 (1994)
 CCC 0021-8995/94/111497-16

process were addressed by experiments with different polymers. This approach had the advantage of demonstrating that the whole method of preparing microcellular foams can be applied to any kind of glassy polymer.

MASS AND HEAT TRANSPORT PHENOMENA OCCURRING DURING THE FOAMING PROCESS OF POLYCARBONATE

Experimental

In recent publications on the production of microcellular glassy polymers, the analysis of the foamed samples focus on the dependence of the number and size of bubbles on preparation parameters such as pressure, temperature, and foaming time. We repeated the experiments with the polycarbonate/CO_2 system with the intention to develop a method determining the glass transition depression of polymer/penetrant system. The PC was kindly supplied as 100 μm thick extruded sheets by DSM/The Netherlands. PC has a glass transition temperature of 150°C and a density of 1.2 g/cm^3.

In preliminary experiments, the PC-sample was saturated at 40 bar CO_2 for 24 h at room temperature. Immediately after pressure release, the sample was dipped into a 100°C glycerol bath for 10 s. Although the bath temperature was well below the glass transition temperature of the pure PC, the sample turned from transparent into nontransparent (opaque) due to the nucleation of bubbles. The foamed samples were washed in a water/ethanol mixture for 1 h, after which the samples were freeze fractured in liquid nitrogen. A scanning electron micrograph of a typical structure is shown in Figure 1.

Remarkably, the specimen shows, besides the bubbles described in the literature, a dense, nonporous layer on the outside of the film and an abrupt transition from the dense layer to the porous structure. This unfoamed skin has been mentioned previously;[5,6] however, no *physical* explanation was proposed for the appearance of this skin. The physical interpretation and the mathematical description presented below explain the appearance of the dense layer and even predict its thickness.

Discussion

As described above, the polymer specimen is saturated in a pressurization step (Figure 2a) at a certain pressure for a fixed time at ambient temperature. During the pressure release step (2b), the polymer sample is exposed to an environment in which the partial pressure of CO_2 is close to zero. Hence, the polymer is supersaturated, and mass transport of CO_2 out of the film takes place. A concentration profile of the penetrant in the film builds up as shown in Figure 2b. The shape of the concentration profile, which actually represents the total penetrant concentration, depends on the length of time the

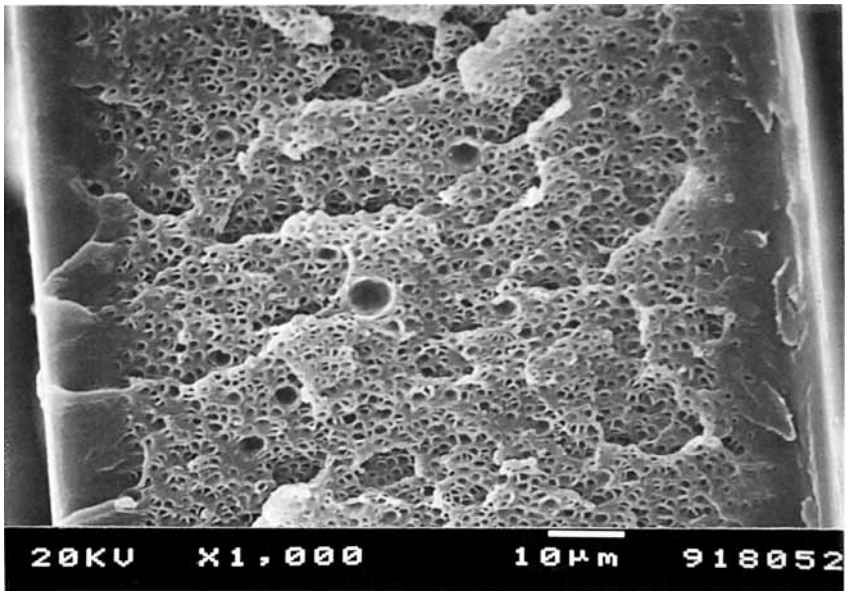

Figure 1 Microcellular polycarbonate foamed after supersaturation with carbon dioxide.

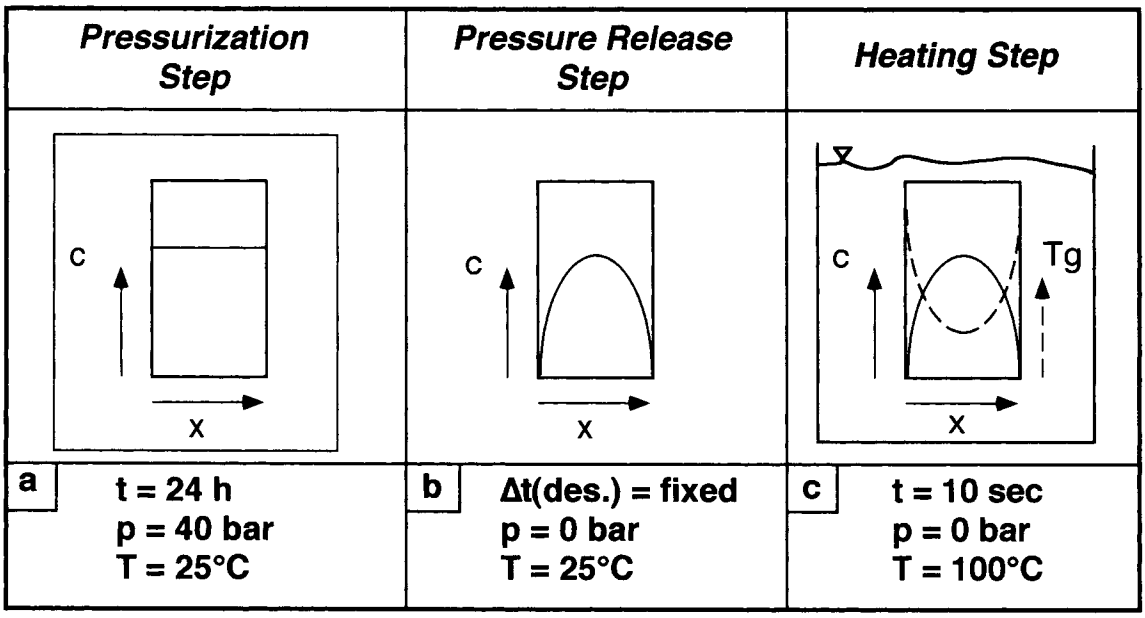

Figure 2 Basic foaming principle showing the individual preparation steps.

sample is kept in this environment. Because any kind of sorbed penetrant lowers the glass transition temperature of a polymer to some extent,[7] a concentration profile in a polymer sample is automatically accompanied by a glass transition temperature profile (2c). Often, a simple emperical relation (1) correlates the glass transition temperature of a polymer/penetrant system with the weight fraction of the penetrant:[8]

$$T_g = T_{g_0} - A \cdot c \qquad (1)$$

where T_g is the actual glass transition temperature of the polymer/penetrant system, T_{g_0} is the glass transition temperature of the polymer free of penetrant, c is the equilibrium concentration of penetrant in the polymer, and A is an empirical plasticization parameter typical for this specific polymer/penetrant system.

A more complex function derived from thermodynamic considerations is also known.[9] However, eq. (1) is adequate to account for the effect of sorbed penetrant molecules on the T_g of the polymer.[10] Kumar[2] observed that foaming is not possible for a polycarbonate sample containing 90 mg CO_2/cm^3 polymer at temperatures below 60°C. Below this temperature, bubbles cannot be created because the polymer is in its glassy state, and the energy barrier for the activation of nucleation is too high. Kumar concluded that this confirms the occurrence of "a significant lowering of the glass transition temperature due to CO_2 sorption." The value of the glass transition observed in this way correlates well with the value of T_g = 65°C, which can be calculated for the same system by applying eq. (1) from Vrentas et al.[8]

The nucleation and growth of the bubbles in the inner part of the specimen is relatively understood; the reasons for the existence of the outer skins are not. To elucidate the formation mechanism, experiments were performed in which the desorption time in the pressure release step is increased. An increased desorption time will result in a lower concentration profile and a related (increased) glass transition profile. If the sample with a certain concentration profile is dipped into the hot glycerol bath, desorption of CO_2 will proceed, but, at the same time, a temperature gradient will build up in the film. On this basis, we hypothesize that exactly at that position in the film where the sample temperature is equal to the glass transition temperature, the abrupt transition from a dense to a porous layer can be observed. Pores can only be formed in that part of the film where the T_g is lower than the local film temperature. For increasing desorption times in the pressure release step, the transition between the dense and porous layer is expected to move towards the middle of the film. Figure 3 shows four polycarbonate samples foamed at the conditions mentioned above. The SEM photos confirm that the transition moves towards the middle of the film.

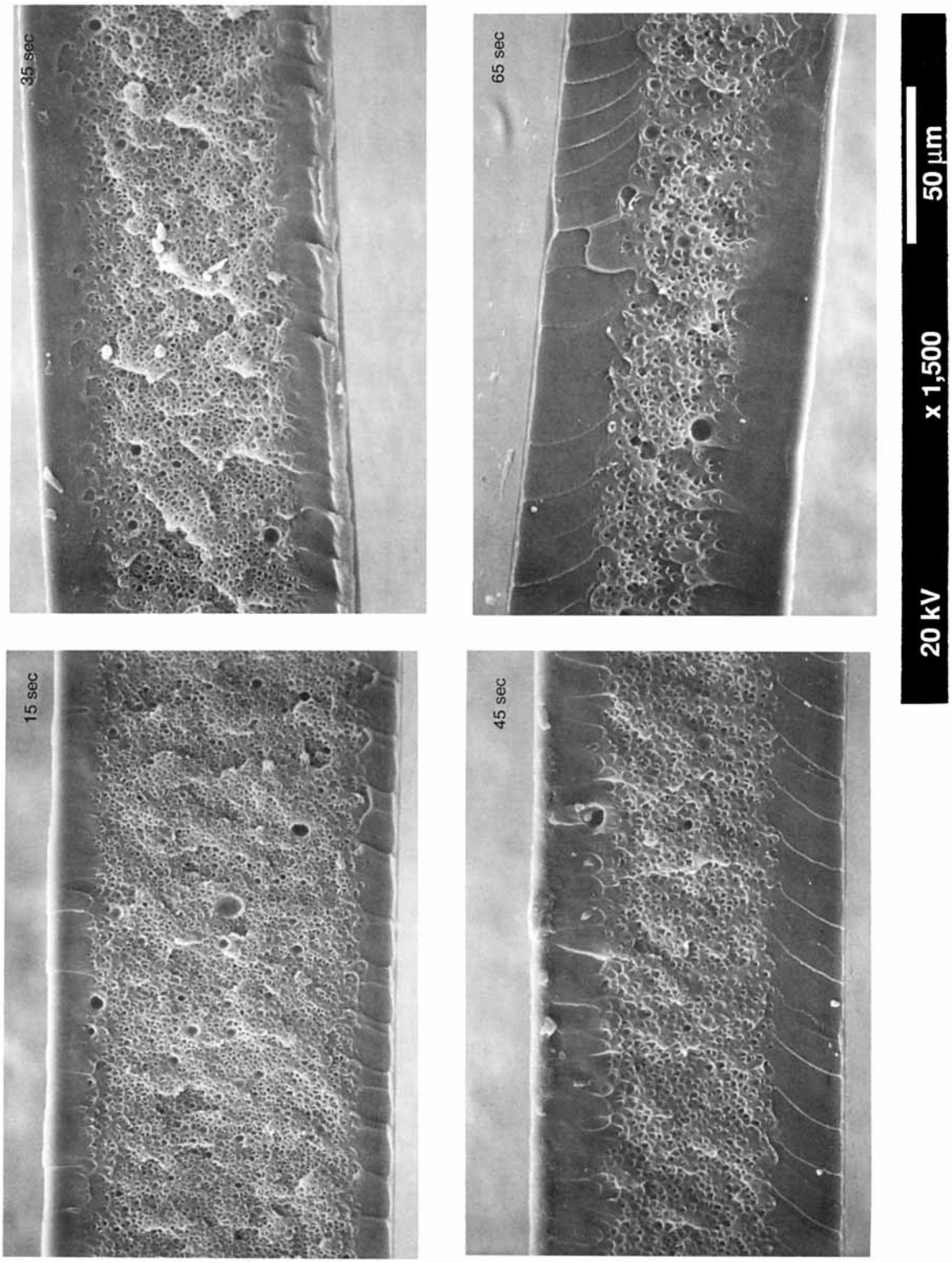

Figure 3 SEM photos of microcellular PC films foamed at different desorption times during the pressure release step.

Table I Variables and Parameters for the Model Calculations

Property	Value	Reference
p_{co_2}	40 bar	
c_{co_2} (40 bar)	44.5 cm^3(STP)/cm^3	13
c_{co_2} (0 bar)	0 cm^3(STP)cm^3	
T_{g0}	150°C	
T_{bath}	100°C	
D_0	0.018 cm^2/s	14
E_D/R	4.5×10^3K	14
D	$1.5 \times 10^{-8}cm^2/s$	*
l	100 μm	
A [in eq. (1)]	1.785	6

* Our experiments; T = 25°C.

Mathematical Modeling of Mass and Heat Transport Phenomena

Mathematically, mass and heat transport phenomena occurring during the different preparation steps of the foam can be described by partial differential equations of the kind

$$\partial u/\partial t = \partial/\partial x(D\partial u/\partial x) \quad (2)$$

where u may be the concentration or the temperature and D the penetrant diffusivity or the termal diffusivity. The partial differential equations describe the evolution of temperature and concentration profiles. The first partial differential equation describes the diffusive transport of the penetrant out of the film during the pressure release step. Here, a constant diffusion coefficient is assumed and the concentration profiles at each time step during the calculations are computed numerically by an FTCS method.[10] The polymer film was subdivided into 500 slices. Further input data for the calculations are listed in Table I. It is assumed for further calculations, that during the heating step in the liquid bath the concentration of CO_2 in the outer layers remains zero and, hence, desorption proceeds. The sample with a concentration profile obtained for a specific desorption time in the pressure release step is now exposed to boundary conditions that characterize the heating step and the second partial differential equation describing the heat transport must be solved. Here, in a first numerical procedure, the heat transport into the film at a fixed time step is calculated. In a second procedure, a diffusion coefficient is calculated as a function of the temperature in each slice according to an Arrhenius relationship

$$D(T) = D_0\exp\{-E_d/RT\} \quad (3)$$

where $D(T)$ is the diffusion coefficient at the local temperature T, D_0 is the diffusion coefficient at infinite temperature and E_d the activation energy of diffusion. A new concentration profile can be calculated with these local diffusion coefficients in a third procedure using the same numerical algorithm as for the pressure release step.

Finally, the glass transition profile at this fixed time step can be calculated from the newly calculated concentration profile by using eq. (1). This T_g profile can be compared with the actual temperature profile in the film as depicted in Figure 4. Because the mass transport is very slow compared to heat transport, the temperature profile (dashed line in Fig. 4) will quickly move closer towards the glass transition temperature profile. The transition layer (which we want to determine) is defined as that slice in the polymer film where the local sample temperature is equal to the local glass transition temperature. This can be evaluated numerically by controlling the sign of the temperature difference between the glass transition temperature and the sample temperature of the specimen at a specific slice. The position of the transition layer depends strongly on the desorption time in the pressure release step. Layer thicknesses are smaller for shorter desorption times $\Delta t_{1,des.}$ shown as position x_1 in Figure 4. For a longer desorption time, the transition moves into the film towards position x_2. To compare the experimental results with the mathematical description, average skin layer thicknesses at both sides of the PC specimen were determined from SEM photos and plotted *vs.* the square root of time[12] in Figure 5.

Because the shift of the transition layer into the film appears to be mass transport limited, a linear relation between the square root of desorption time and the experimental layer thickness is be expected. Indeed, the linear relation can be observed as shown in Figure 5. Even the mathematical model fits the experimental data well, confirming the physical and mathematical picture above. For short desorption times, the experimental data fit the model calculations very well. At longer desorption times, the layer thicknesses for both sides of the film diverge. This might be caused by different polymer chain packing densities in the film, depending on the thermal history during the extrusion process. In fact, history effects such as orientation and residual stress can only be observed at the outer skin because the skin is still in its glassy state. The transition from the glassy state to the rubbery state, as occurred between the skins, deletes such history effect.

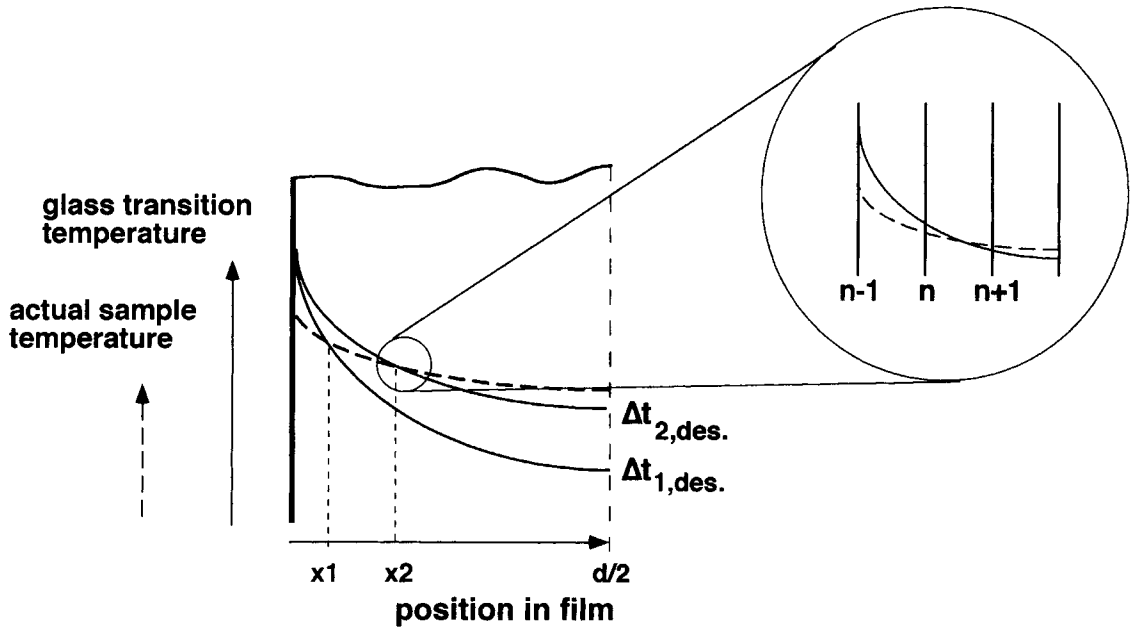

Figure 4 Temperature and glass transition temperature profiles as a function of the desorption time: $\Delta t1$ for desorption in the pressure release step is smaller than $\Delta t2$.

Nodular Structure

A closer look at the cross-section of the homogeneous, dense outer layers of the foamed specimen reveals a peculiar structure. The layer is not dense and homogeneous, as it was before the foaming experiment. As can be seen in the SEM photos given in Figure 6, the outer layer shows a nodular structure.

To investigate at which step in the process the nodular structure occurs, the preparation procedure was stopped at different stages, and the sample was analyzed by SEM. No nodules can be observed before the saturated sample is exposed to the heating step in the hot glycerol bath, which confirms that the nodules are not artefacts introduced by the preparation techniques for the SEM analysis.

Nevertheless, the influence of sample preparation conditions for the SEM analysis was also investigated. The samples are normally sputtered with gold at an argon pressure of 0.1 torr for around 3 min at a current of 15 mA with the specimen 55 mm un-

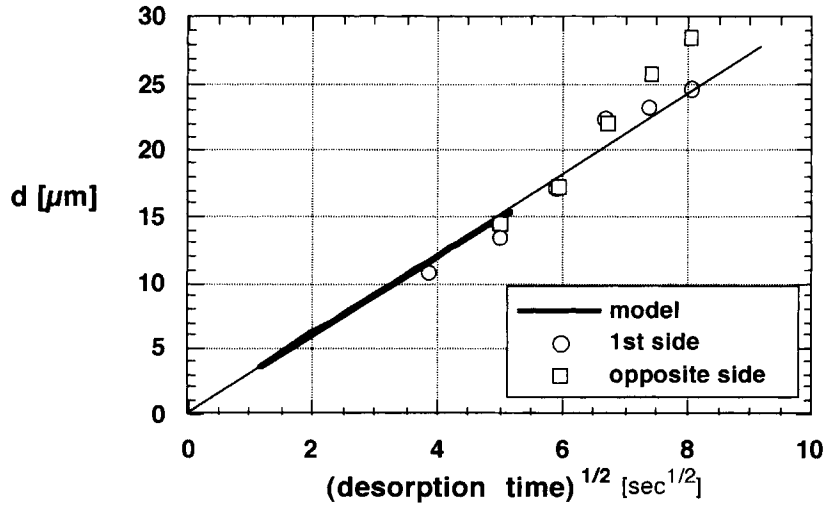

Figure 5 Comparison of model calculation with experimental skin layer thicknesses.

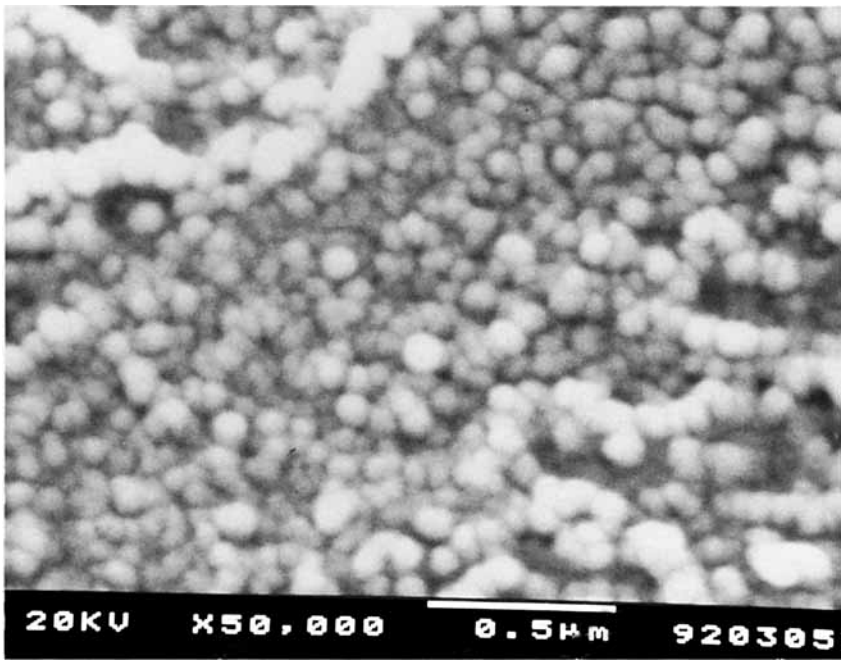

Figure 6 SEM photo of the nodular structure found in the cross-section of the skin layer of a microcellular polycarbonate sample.

derneath the gold electrode. Sometimes, gold deposition on a smooth inorganic glass surface results in a nodular structure, but the nodule size then becomes zero upon extrapolation to zero sputter time.

The same PC sample was sputtered step wise for different sputter times. Between two sputter steps, the nodule size was measured on SEM photos, always at the same position of the fracture surface of the specimen. With increasing sputter time the size of the nodules in the cross-section of the nonporous outer layer of the PC specimen increased, as shown in Figure 7. From the slope of the curve, an average deposition rate can be calculated, which actually meets the specification of the apparatus well. Extrapolation to zero sputter time results in the actual nodule size of 40 nm.

Atomic force microscopy (AFM) was used to reconfirm and to illustrate in more detail this peculiar

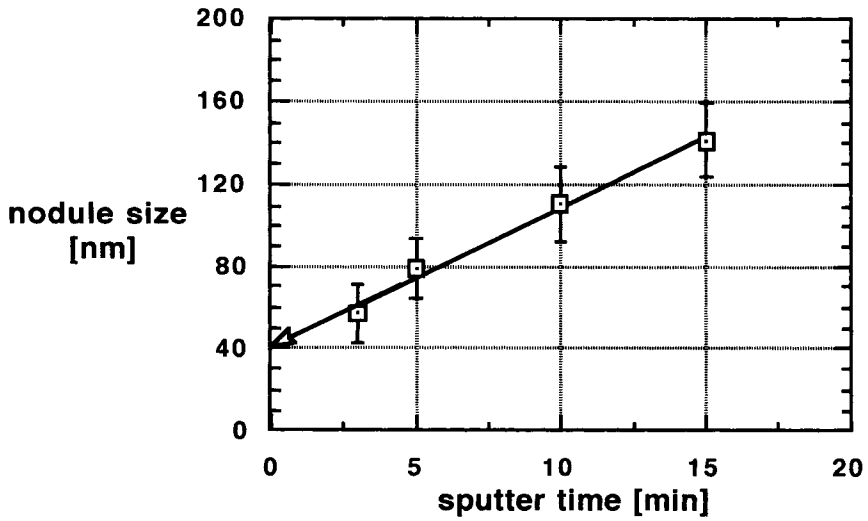

Figure 7 Nodule size, depending on the sputter time.

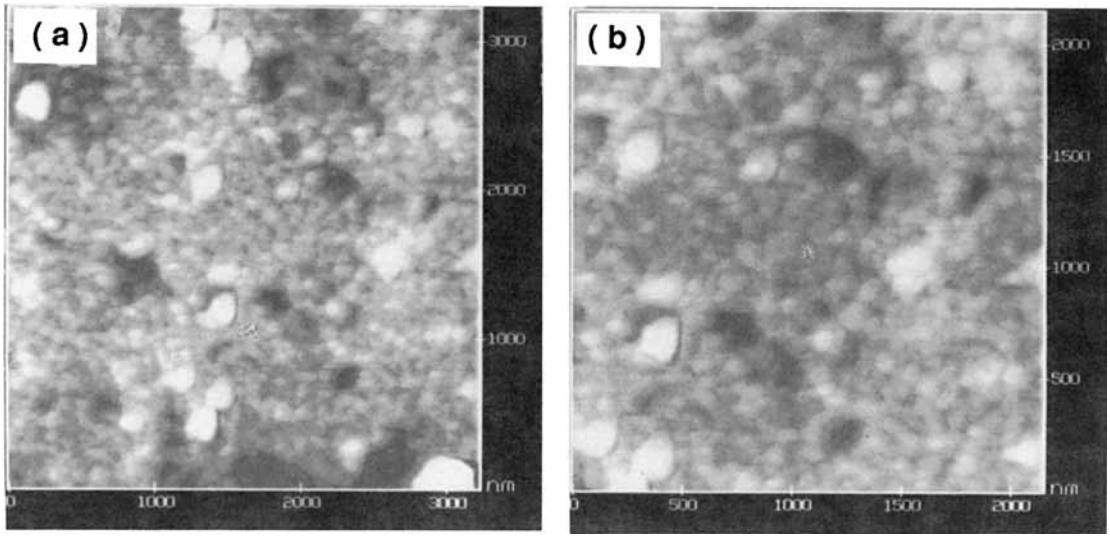

Figure 8 Atomic force microscopy photo of the nodular structure of the skin layer; picture size represents a surface of (a) 3 μm $\times$ 3 μm and (b) 2 μm $\times$ 2 μm.

structure. No such structure was found in untreated samples. After foaming, a grainy nodular structure was found in the cross-section of the dense outer layer, as shown in Figure 8. Here, the nodule size is in the range of 50–200 nm. The discrepancy between the AFM and the SEM photos might be caused simply by the fact that the AFM-analyzed surfaces do not represent the small part of the layer observed in the SEM photo. In fact, with the AFM used, it was hardly possible to focus on a specific surface area of the specimen.

The physical reasons for the creation of these nodules are not obvious. From Figure 6, it *seems* as if the nodular structure is built out of ball-like entities with voids in between. However, the creation of such spherical surfaces would be very energy intensive because of the disentanglement of the dense, glassy polymer matrix. Sufficient energy might be supplied by the high temperature of the heating step and the extraordinarily high supersaturation. On the other hand, nodules in amorphous dense polymer films have been reported by Yeh[15] and Geil.[16] The occurrence of these nodules in amorphous polymers and the tendency of amorphous polymers to crystallize upon heat treatment lead to the development of the model of Yeh.[17] This model describes local ordering by the folded-chain, fringed micellar grain model, which is actually a type of bundle model.[18] Bundle models generally assume small ordered regions, showing strong, narrow distance correlations with superimposed disordered regions, showing very broad distance correlations.

The nodular structures reported by Geil are small in size and generally have a diameter of around 30Å. These nodules can aggregate into "super-nodules" depending on the thermal history of the sample, because aggregation of nodules may minimize their intergrain surface energy. Both heat treatment and

	Tg (°C)	density (g/l)	molecular mass (g/mol)
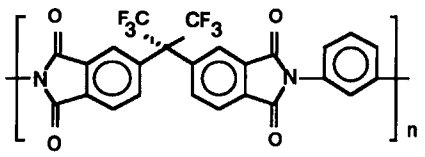	313	1.467	516.4

Figure 9 Chemical structure and physical properties of the aromatic polyimide 6FDA-3PDA.

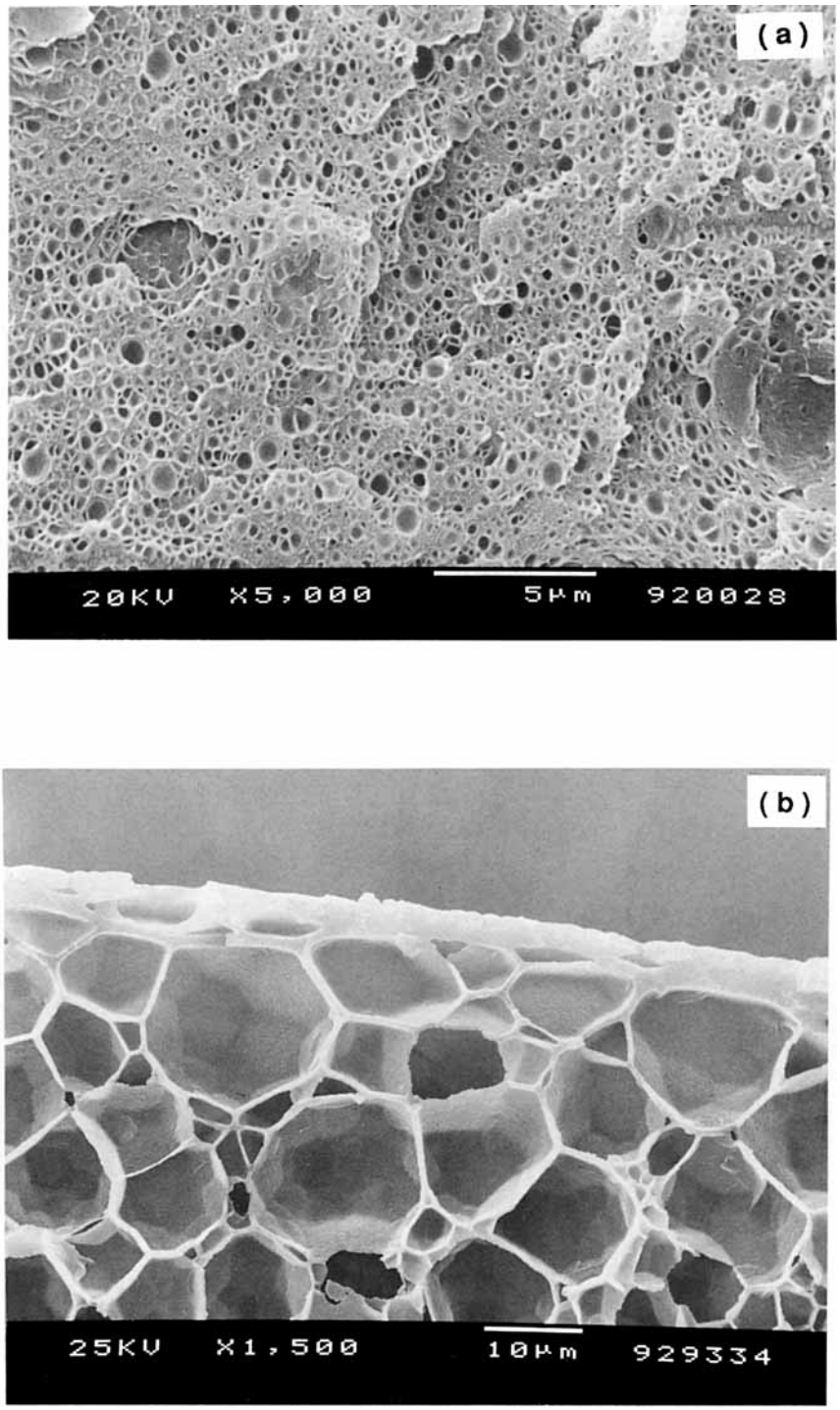

Figure 10 Microporous polyimide foamed by carbon dioxide at (a) p_{co_2} = 35 bar and T = 135°C and (b) p_{co_2} = 20 bar and T = 220°C.

CO_2-sorption have the potential to enhance ordering phenomena, e.g., crystallization in amorphous PET.[19] It seems reasonable, therefore, that, during the preparation of the microcellular foams, the polymer sample experiences such extreme conditions, i.e., high penetrant concentration and high temperature, that the creation of such "super-nodules" out of areas of enhanced local ordering in the

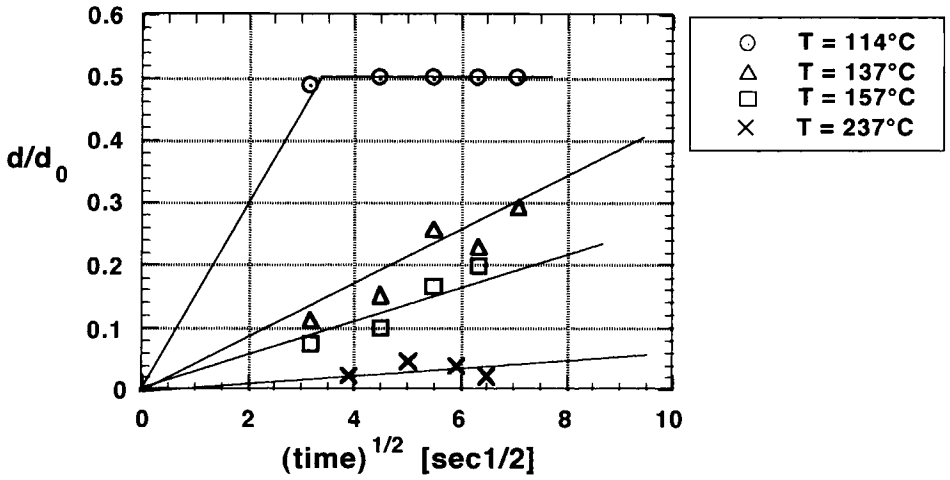

Figure 11 Thickness of the dense layer depending on the desorption times in the pressure release step at different foaming temperatures and a saturation pressure of p_{co_2} = 50 bar.

sense of bundle models may be favorable. At this stage, no definite decision on the validity of either physical interpretation can be made. Future work, such as permeation experiments, which would give information on the density and eventually porosity of the toplayer, are required to elucidate this problem.

SORPTION-INDUCED GLASS TRANSITION TEMPERATURE DEPRESSION OF A POLYIMIDE

Polyimides are polymers with outstanding thermal, mechanical, and chemical properties. A family of polyimides based on the hexafluoro-dianhydride unit 6FDA [4,4'-(2,2,2-trifluoro methyl)ethylidene]-bis[1,3-isobenzofuran-dione]) has attracted considerable interest in the last 5 years in the field of membrane technology. These polymers show high permeabilities and high selectivities for gas mixtures. However, highly sorbing penetrants such as CO_2 swell the polymer significantly and reduce the selective properties. Relaxation phenomena occur in the form of time-dependent gas permeabilities and swelling volumes.[4] These phenomena are generally summarized in the term plasticization. Because plasticization can be related to a depression of the glass transition temperature, the extent to which the T_g of a polyimide, which might be used as a membrane material, is depressed by the presence of sorbed CO_2 is of general interest. Most of the methods determining the T_g depression described in literature, however, are not very suitable or are even impracticable for polymers with glass transition temperatures higher than 200°C. The method described in the first part of this article is very easy to use and might be suitable for this purpose.

The polyimide used is 6FDA-3PDA; the chemical structure, physical characteristics, i.e., density, molar mass, and glass transition temperature are shown in Figure 9. Films of around 100 μm thickness were cast from a 20% weight DMAc solution. The solvent was evaporated in a nitrogen-flushed glove box. The films were then dried in a vacuum oven at 70°C for at least 1 month to ensure the complete removal of residual solvent. The foaming experiments were carried out in the same way as those described above.

Not only was the desorption time in the pressure release step varied, but also the bath temperature and the applied pressure. Depending on the difference between the bath temperature and the actual $T_g(p)$, different foam structures can be obtained, as shown in Figure 10. In general, the average cell diameter increases with increasing bath temperature at a constant saturation pressure.[2] Figure 10a shows a foam structure in which small spherical pores, 0.5 μm in diameter, are embedded in a solid polymer matrix. In the sample shown in Figure 10b, large honeycomb-like pores, 10 μm in size, are separated by thin walls of polymer matrix.

In a new experimental series, the desorption time was varied at different bath temperatures. The thickness of the dense, outer layer was measured and was plotted normalized for the initial film thickness vs. the square root of the desorption time in Figure 11. In this figure, the normalization of the layer thickness was chosen, since a maximum value of 0.5 for d/d_0 means that no foaming occurs in the specimen.

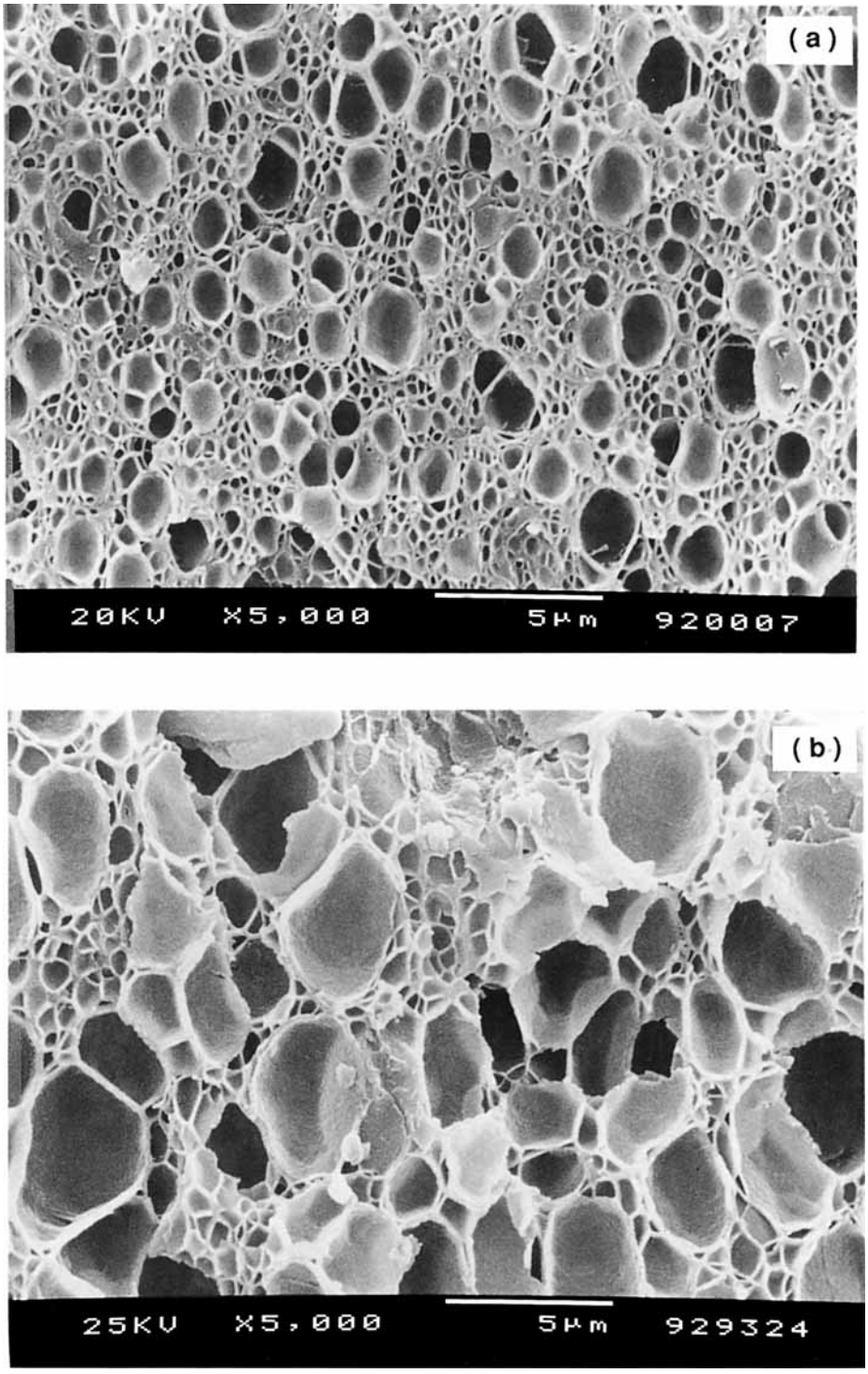

Figure 12 Polyimide microcellular foams showing bimodal bubble size distributions foamed at p = 35 bar and different temperatures: (a) T = 169°C and (b) T = 175°C.

For bath temperatures of 137, 157, and 237°C, respectively, the samples always show a microcellular structure for the desorption times investigated. At 114°C, however, no foaming could be observed after desorption times of about 15 s. Hence, the T_g drops from initially 312°C to *at least* 114°C at a saturation pressure of 50 bars. During the experiments it was clearly seen that the samples that were

foamed at 114°C with a saturation pressure of 50 bars did not turn opaque for desorption times larger than 20 s. For these desorption times, the glass transition temperature of the sample was always larger than the bath temperature.

It is, therefore, possible to observe the glass transition temperature depression by systematically decreasing the bath temperature, even without using a scanning electron microscope. The temperature at which no foaming occurs (the sample does not undergo a transparent/opaque transition) is then the actual glass transition temperature of the polymer/penetrant system.

The SEM analysis of the polyimide microcellular foams revealed another phenomenon that has not been mentioned previously in the literature. Under certain preparation conditions, the foam will show a bimodal bubble size distribution, as shown for two different samples in Figure 12.

The striking characteristic is that the second series of smaller bubbles lies between larger bubbles belonging to the first population. This phenomenon is explained by the fact that the nucleation of bubbles starts at a time $t = t_0$, while new nuclei are formed and grow out to bubbles as time proceeds. This can be described by eq. (4):[20]

$$F(t) = F_0 \exp\left(-\frac{\tau}{t}\right) \tag{4}$$

in which τ is a measure of the transient time necessary to reach the equilibrium nucleation frequency, F_0, and $F(t)$ is the time-dependent nucleation frequency characterizing the number of nuclei formed per time and volume unit. Let us consider a polymer/penetrant phase that starts to form a number of nuclei continuously in time and let us furthermore assume that this continuous process can be idealized as a finite sum of discrete time steps at which new generations of nuclei will be formed. The continuous function for the ratio of $F(t)/F_0$ can then be approximated by discrete steps in the number of nuclei.

A first generation will grow in time and subtract gas from its surrounding. Now, a "second generation" nuclei develops that also can grow. The second generation, however, cannot grow as much as the first generation because of the lower concentration of penetrant in the polymer matrix. This process of nucleation will continue, but, as soon as the penetrant concentration reaches a critical concentration at which the corresponding glass transition temperature is equal to the sample temperature, no further nucleation and growth can occur. (If this were not the case, the described mechanism would result in a perfect self-similar, fractal foam morphology.)

From the SEM photos in Figure 12, it can also be seen that more small pores exist than larger ones. This is in accordance with the prediction of eq. (4), that is, in the early stages of nucleation, the number of nuclei formed at later times must be larger than the number of nuclei formed in the early times. However, at this point, it is not known whether nucleation actually occurs homogeneously or heterogeneously. This will be worked out in more detail in the following section.

TRACING THE GLASSY STATE OF A POLYSULFONE BY NUCLEATION OF GAS BUBBLES

Cell nucleation in the amorphous rubbery phase is assumed to be homogeneous in nature[2] following an Arrhenius type of relation for the nucleation rate n_{hom}

$$n_{\text{hom}} = c_0 f_0 \exp\left\{\frac{-\Delta G}{kT}\right\} \tag{5}$$

where c_0 is the concentration of the sorbed gas molecules in the polymer, f_0 the frequency factor for gas molecules joining the nucleus, k Boltzman's constant, T the foaming temperature, and ΔG the activation energy for nucleation. The activation energy ΔG obeys eq. (6):

$$\Delta G = \frac{16\pi\gamma^3}{3(p_s - p_0)^2} \tag{6}$$

where γ is the surface energy between the polymer and the gas phase, p_s the saturation pressure during the pressurization step and p_0 the environmental pressure at which the foaming will be carried out. Equation (5) predicts that a temperature increase should cause a drastic increase of the number of bubbles formed in the polymer. Experimentally, Kumar found contradictory results: the nucleation rate was independent of the foaming temperature. This lead to the conclusion that traditional theories on homogeneous nucleation are clearly not applicable. However, it was not suggested that nucleation may also occur in a heterogeneous manner.

Considering the glassy polymer phase as having a free-volume distribution, heterogeneous nucleation

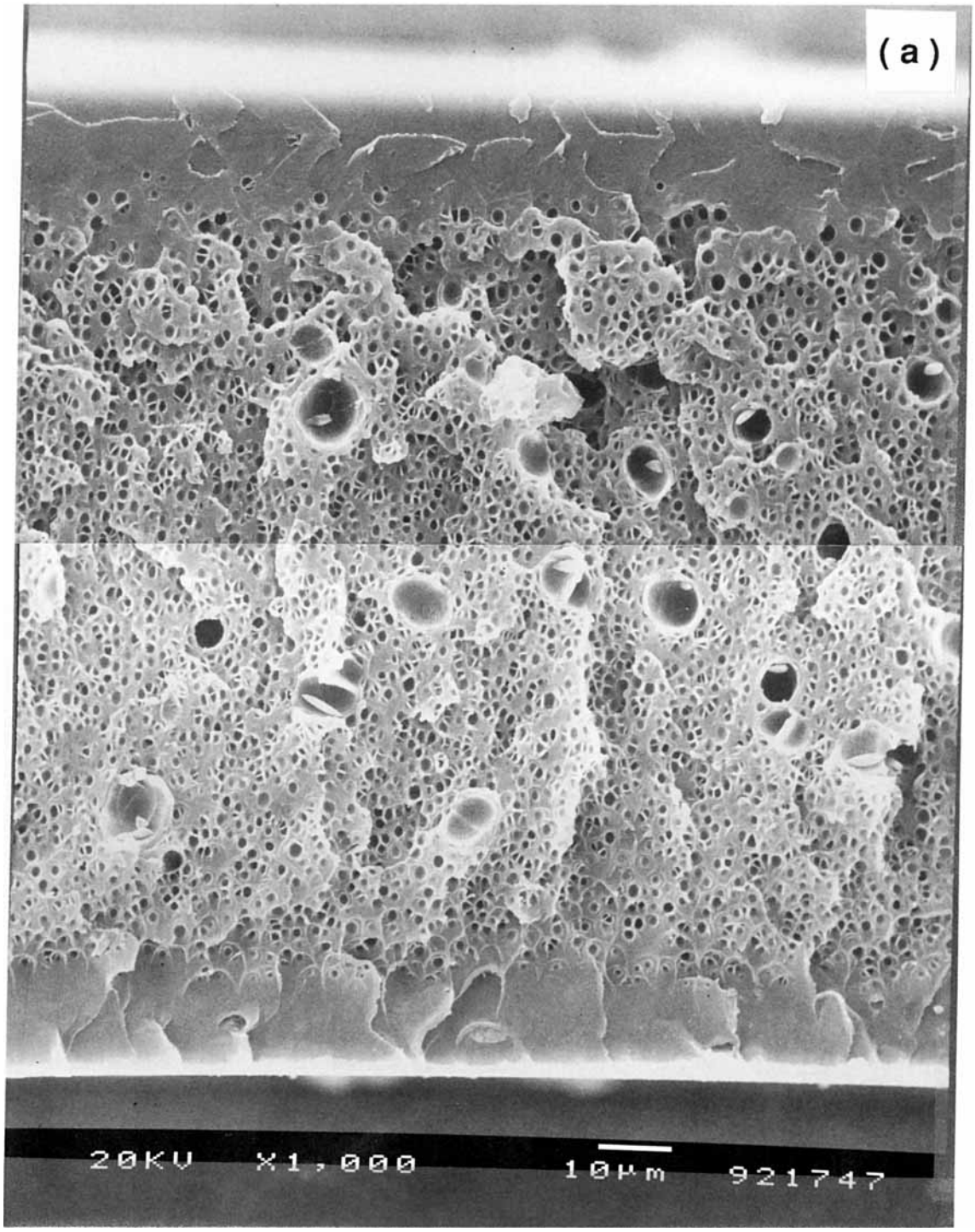

Figure 13 Microcellular polysulfone foamed at the same preparation conditions; the samples have, however, different thermal histories: (a) quenched from the glassy state, (b) slowly cooled down through the glass transition region.

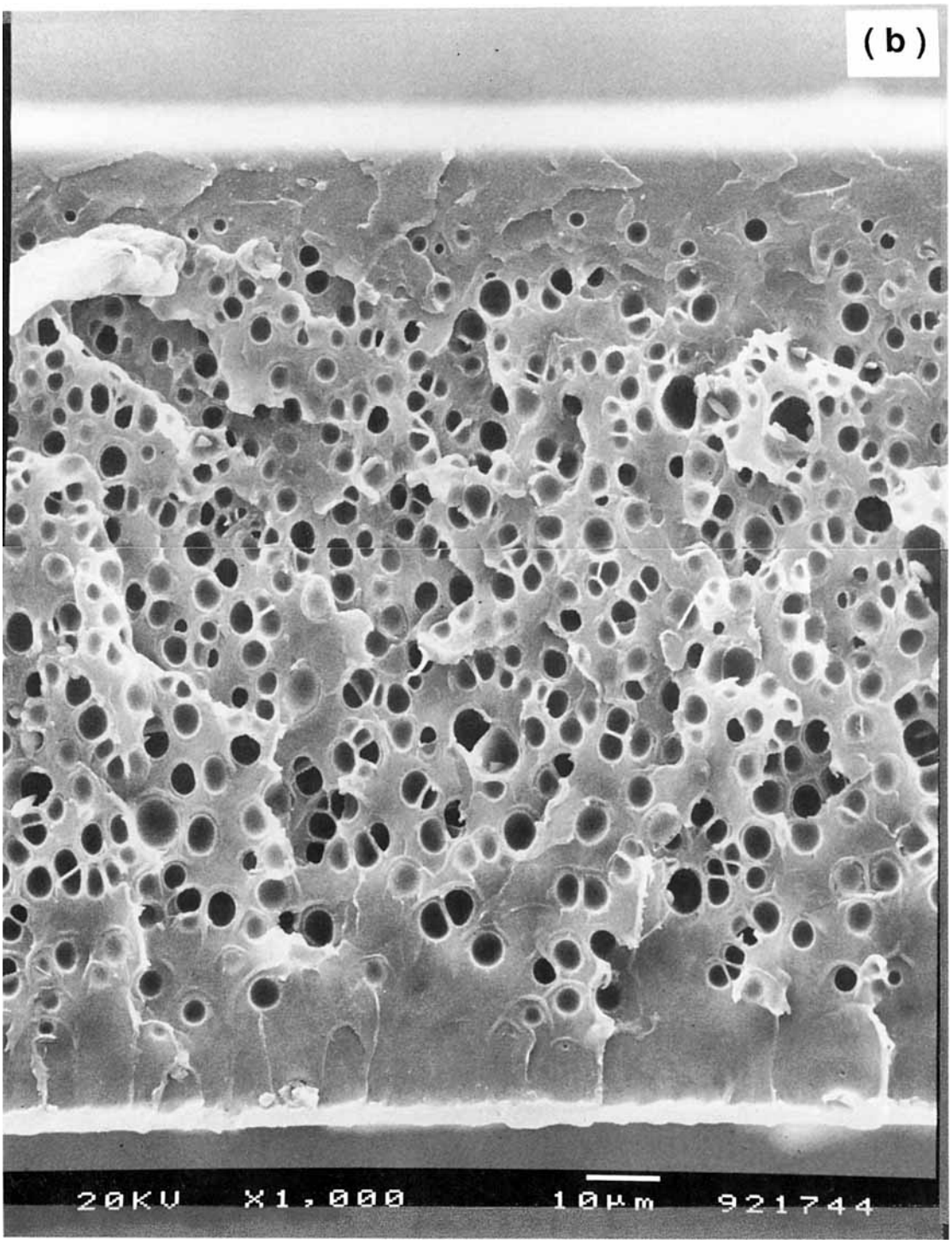

Figure 13 (*Continued from previous page*)

is not unrealistic. Free-volume or density fluctuations are frozen into the polymer matrix during the glass formation. The larger free-volume pockets may already exist in the matrix in such an energy state that only slight "internal" pressure is needed for growth into bubbles.

Experimentally, this idea of heterogeneous nucleation in loci of larger frozen-in density fluctua-

tions can be confirmed by carrying out annealing experiments. On cooling, thermal density fluctuations of a rubbery polymer are frozen in at the glass transition temperature. At much lower temperatures than T_g the polymer will densify very slowly. These relaxational densification processes can be enhanced if the polymeric glass undergoes a heat treatment at a temperature just below T_g. Such a heat treatment results in a much more homogeneous polymer matrix, with fewer loci where heterogeneous nucleation can occur easily.

To test this *hypothesis* of heterogeneous nucleation at frozen-in density fluctuations, the following experiments where carried out. Polysulfone samples (cast from a DMAc solution, 100 μm thick, T_g = 190°C) were heated above the glass transition temperature at 204°C for 20 h. They were then briefly quenched in water at 20°C. Two samples were heated again at 204°C. One of the samples was quenched directly in liquid nitrogen, whereas the other one remained in the oven. The oven was switched off and cooled down slowly to 50°C within 6 h. In the first sample (A), essentially the density fluctuations of the rubbery state are frozen in. The second sample (B) can be considered as an annealed sample because it undergoes a very slow glass formation process. From the above-mentioned theoretical considerations, sample A should have a higher bubble density than sample B after foaming. Cross-sections of the two samples, foamed at 140°C and a saturation pressure of p = 40 bar CO_2, are shown in Figure 13 (other foaming parameters are the same as before).

Clearly, the number of bubbles in sample A is significantly larger than in sample B, supporting the idea of heterogeneous nucleation at frozen-in density fluctuations. Table II shows the results of the counting analysis of the pictures. Besides the two samples shown in Figure 13, table II also contains data on a sample (C) that did not undergo the second heat treatment at 204°C (i.e., a water quenched sample after one heating step). In fact, due to the essentially identical quench conditions, the number of bubbles in sample A and C are almost equal.

Table II Influence of the Thermal History of the Polymer Film on the Bubble Density of CO_2 Foamed PSF at T = 140°C and p_{co_2} = 40 bar

Sample	Number of Bubbles (l/mm^2)
A	2.02 E+05
B	0.32 E+05
C	1.68 E+05

CONCLUSIONS

The nucleation of gas bubbles in homogeneous polymer films supersaturated with CO_2 was used to develop a simple method for the investigation of the T_g depression due to the sorption of penetrant molecules. The physical picture proposed, together with the mathematical model, describes very well the observed macroscopic structure, consisting of a porous inner layer enclosed by interfacial dense layers. The method was used to investigate the T_g depression of a polyimide, which was saturated with CO_2 at 50 bars. A considerable drop in the glass transition from T_{g_0} = 312°C to T_g = 114°C was observed demonstrating clearly the plasticizing effect of this penetrant.

A nodular structure in the outer, dense layers of the foamed sample was observed using SEM. This structure was confirmed by atomic force microscopy. Two interpretations are suggested: (a) the nodules are formed by density segregation necessitating a disentanglement of the glassy polymer matrix, or (b) the nodules grow out of regions of enhanced local ordering following the physical picture of bundle models. No definite decision for either interpretation can be made.

Foaming experiments with polysulfone samples having different thermal histories suggest that the nucleation mechanism underlying the foaming process is heterogeneous in nature. Loci of nucleation are the larger free-volume pockets, that are embedded in a more densified polymer matrix.

REFERENCES

1. J. E. Martini, N. P. Suh, and F. A. Waldman, U.S. Pat. 4,473,665 (1984).
2. V. Kumar and J. E. Weller, *ANTEC*, 1401 (1991).
3. M. L. Williams, R. F. Landel, and J. D. Ferry, *J. Am. Chem. Soc.*, **77**, 3701 (1955).
4. M. Wessling, S. Schoeman, Th. v. d. Boomgaard, and C. A. Smolders, *Gas Sep. Purif.*, **5**, 222 (1991).
5. V. Kumar, Ph.D. Thesis, Massachusetts Institute of Technology, 1988.
6. S. B. Hadenbrook, L. P. Harasta, S. T. Falkenberry, and R. D. Bomba, U.S. Pat. 4,761,256 (1988).

7. J. H. Gibbs and E. A. DiMarzio, *J. Chem. Phys.*, **28,** 373 (1958).
8. J. S. Vrentas and C. M. Vrentas, *Macromolecules,* **24,** 2404 (1991).
9. T. S. Chow, *Macromolecules,* **13,** 362 (1980).
10. H. Hachisuka, T. Sato, T. Imai, J. Tsujita, A. Takizava, and T. Kinoshita, *Polymer J.*, **22,** 77 (1990).
11. W. H. Press, B. P. Flannery, S. A. Teukolsky, and W. T. Vetterling, *Numerical Recipes,* Cambridge University Press, Cambridge, 1989.
12. J. Crank, *Mathematics of diffusion,* Cleardon Press, Oxford, 1975.
13. G. K. Fleming and W. J. Koros, *J. Polym. Sci., Polym. Phys.*, **28,** 1137 (1990).
14. D. W. van Krevelen, *Properties of Polymers,* Elsevier, Amsterdam, 1990.
15. G. S. Y. Yeh, *J. Macromol. Sci.-Phys.*, **B6(3),** 451 (1972).
16. K. Neki and P. H. Geil, *J. Macromol. Sci.-Phys,* **B8(1–2)** 295–341 (1973).
17. G. S. Y. Yeh, *J. Macromol. Sci.-Phys.*, **B6(3),** 465–478 (1972).
18. I. Voigt-Martin and J. Wendorff, in *Encyclopedia of Polymer Science and Engineering,* Vol. 1, J. Wiley & Sons, New York, 1985.
19. K. Mizoguchi, T. Hirose, Y. Naito, and Y. Kamiya, *Polymer,* **28,** 1298 (1987).
20. A. G. Walton, in *Nucleation,* A. C. Zettlemayer, Ed., Marcel Dekker, New York, 1969, p. 225.

Received September 24, 1993
Accepted February 25, 1994